Journal of Heat and Mass Transfer Research

Journal homepage: https://jhmtr.semnan.ac.ir

Semnan University

ISSN: 2383-3068

Research Article

Chemical Reactions on MHD Couple Stress Fluids towards Stretchable Inclined Cylinder

Suman Sharma *, **Shalini Jain**

Department of Mathematics, University of Rajasthan, Jaipur-302004, India

ARTICLE INFO

Article history:

Received: 2023-07-12

Revised: 2024-04-04

Accepted: 2024-04-05

Keywords:

Couple stress fluid;

MHD;

Nonlinear convection;

Porous media;

Homogeneous – Heterogeneous reaction.

ABSTRACT

This study focuses on exploring the influence of homogeneous and heterogeneous chemical reactions on a couple of stress fluids surrounding a permeable inclined stretching cylinder. The impact of a uniform magnetic field and porous media is also considered in the fluid model. It is assumed that the diffusion coefficients for chemical species A and B are of similar magnitudes and that the heat released during the chemical reaction is negligible. The governing partial differential equations (PDEs) are evolved and transformed into ordinary differential equations (ODEs) using adequate similarity alterations. These ODEs are subsequently solved using the shooting technique in conjunction with the fourth-order Runge-Kutta method, implemented through MATLAB software. Results are presented through graphs and tables depicting the velocity, temperature, and concentration fields. Furthermore, numerical findings for the skin friction coefficient and Nusselt number are discussed. The concentration field experiences a decline as homogeneous-heterogeneous reactions intensify, attributable to the heightened dispersion of concentrations across the system, resulting in a more intricate distribution pattern.

1. Introduction

Couple stress pertains to the internal forces within a fluid resulting from the distortion of fluid elements. These forces are associated with the swirling motion of fluid particles and can influence the overall fluid behavior. Fluids comprising rigid, randomly dispersed particles within a viscous example being blood, lubricants with minimal polymer additives, electro-rheological fluids, and synthetic fluids exhibit such size-dependent effects. Stokes [1] introduced a couple of stresses in viscous fluids, emphasizing the presence of size-dependent effects determined by the material constant and dynamic viscosity, a factor absent in traditional viscous theories. Rani et al. [2]–[4], Ibrahim, and Gadisa [5]scrutinized the dynamics of couple stress fluid flow around a vertical cylinder. Gajjela and Garvandha [6] delved into the effects of chemical reactions on a couple of stress fluids through a stretching cylinder. Palaiah et al. [7] scrutinized the influence of thermal radiation on magnetized couple stress fluid flowing over a vertical cylinder. Asad et al. [8] investigated heat transfer with variable thermal conductivity in a couple of stress fluids over an inclined stretching cylinder. Khan et al. [9] derived an exact solution for the flow of magnetohydrodynamic (MHD) couple stress fluid. Bharty et al. [10] analyzed the influence of chemical reactions and magnetic fields on the onset of double-diffusive convection

* **Corresponding author.**
E-mail address: *s9549170542@gmil.com*

Cite this article as:
Sharma, S. and Jain, S., 2024. Chemical Reactions on Mhd Couple Stress Fluids towards Stretchable Inclined Cylinder. *Journal of Heat and Mass Transfer Research*, 11(1), pp. 139-150.
https://doi.org/10.22075/JHMTR.2024.31241.1463

within a couple stress fluid confined between elongated parallel plates.

The significance of chemical reactions extends widely across industrial and practical domains. Certain processes involving chemical reactions exhibit a combination of both reactions, such as those found in combustion, biochemical systems, etc. Notably, these reactions can either cease or proceed even without the Occurrence of a catalyst. The interplay between these reactions on catalytic surfaces is remarkably complex, involving varying production and consumption rates within the fluid medium. Many researchers, such as Malik and Khan [11], Rashad et al. [12], Giri et al. [13], and Hayat et al. [14], examined chemical reaction impact over various geometries. Jain and Gupta [15] studied chemical reactions past stretching sheets with suction and injection impacts. Narayana et al. [16] investigated the impact of homogeneous-heterogeneous reactions on a couple of stress fluids over a stretching sheet. Naveed et al. [17] investigated the flow of a couple of stress fluids in the grip of chemical reactions past a stretchable sheet. Rana et al. [18] analyzed a couple of stress fluid flows past a Riga plate regarding the effectiveness of chemical reactions. Swapna et al. [19] elucidated the flow of Casson nanofluid in the presence of a chemical reaction coefficient flowing past a linearly stretching surface. Kumari and Jain [20] studied the impact of chemical reactions on Casson fluid. Parmar and Jain [21] investigated chemical reactions past three vertical surfaces.

The study of heat transfer over an inclined stretching surface has garnered attention from numerous researchers due to its diverse applications in industry and technology. This phenomenon is extensively used in wire drawing, fire production, glass fiber manufacturing, and hot rolling processes. Many researchers, Abbas et al. [22], Awan et al. [23], and Sohail and Naz [24], examined the influence of fluid flow and heat transfer over a stretched cylinder. Mabood et al. [25] studied the convective flow of a couple of stress fluids with thermal radiations. Afzal et al. [26] investigated the double-diffusive convection of a couple of stress fluids into a channel. Prasad et al. [27] investigated the flow of couple stress fluid under convective boundary conditions. Mahat et al. [28] studied the mixed convective flow of viscoelastic fluid past a cylinder. Usman et al. [29] observed the heat and mass transfer phenomena in the radiation and activation energy influences on a horizontal porous plate. Fatima et al. [30] investigated the thermal and mass transfer characteristics of viscous fluid flow influenced by buoyancy forces within a channel. Huang et al. [31] investigated mass and heat transfer flow comprising two immiscible fluids driven by ciliary motion within a channel. Arain et al. [32] examined the bioconvection of nanofluid flowing between parallel plates in the influence of activation energy.

Magnetohydrodynamics (MHD) is essential for a wide array of phenomena, spanning from astrophysical events like solar wind behavior to practical applications such as metal manufacturing, stabilizing fusion processes, refining medical practices like magnetic drug delivery, and enhancing airflow control. Reddy et al. [33] analyzed the impact of heat transfer on MHD fluid flow through a stretching cylinder. Sudarmozhi et al. [34] studied the MHD flow of Maxwell fluid past a stretching cylinder. Hussain et al. [35] analyzed the MHD flow of Williamson fluid with a chemical reaction over a sheet and cylinder. Arain et al. [36] analyzed the flow of Sutterby fluid with the induced magnetic field in the presence of motile gyrotactic microorganisms. Sekhar et al. [37] investigated the dynamic heat and mass transfer on MHD convective flow past an infinitely porous plate.

After reviewing the existing literature, it can be concluded that the characteristics of MHD couple stress fluid with the influence of homogeneous and heterogeneous reactions over an inclined stretching cylinder have not been thoroughly investigated thus far. Consequently, this paper aims to fill this research gap by examining the impact of homogeneous and heterogeneous reactions on a couple of stress fluids past an inclined stretching cylinder in the presence of a porous medium and magnetic field. It is assumed that the diffusion coefficients for species A and B are of similar magnitude. The governing PDEs are evolved and transformed into ODEs using adequate similarity alterations. These ODEs are subsequently solved using the shooting technique in conjunction with the fourth-order Runge-Kutta method, implemented through MATLAB software. The results are presented through graphical representations illustrating the velocity, temperature, and concentration fields.

2. Mathematical Formulation

Consider a two-dimensional flow of steady, incompressible, viscous flow of non-Newtonian fluid with homogeneous–heterogeneous reaction over an inclined stretchable cylinder. This study aims to explore heat transfer analysis under the effect of couple stresses. The x-axis aligns with the cylinder's axis, while the r-axis is normal to it. The cylinder is stretching at a velocity given by $u_w(x) = \frac{U_0}{lx}$, where U_0 is the reference velocity, and l is the characteristic length. The cylinder's inclination is represented by α. A uniform

magnetic field B_0 is also applied along the r-direction. The surface maintains constant temperature and concentration, denoted as T_w and C_w, respectively. At a distance far from the boundary, these values are represented by T_∞ and C_∞, respectively.

A basic model for reactions, both homogeneous and heterogeneous, within a boundary layer flow was introduced by Chaudhary and Merkin [38]. We consider isothermal cubic autocatalytic kinetic (homogeneous) within the boundary layer flow given by

$$A + B \to 3B, \ \text{rate} = l_1 ab^2 \tag{1}$$

and single first-order kinetics (heterogeneous) on the catalyst surface as

$$A \to B, \ \text{rate} = l_s a \tag{2}$$

here, a and b are concentrations of A and B chemical species and l_1 and l_s are constant. a_0 is the constant concentration of A. The rate of reaction at the outermost edge of the boundary layer will be zero. In the external flow B there is no auto catalyst.

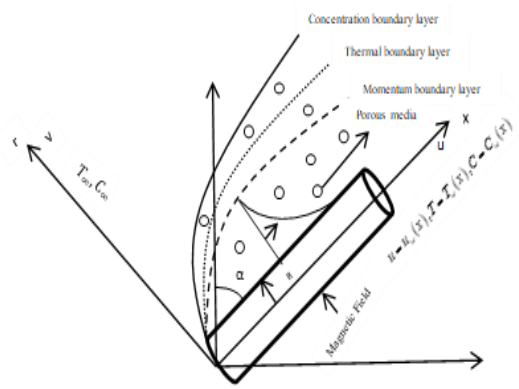

Fig. 1. Diagram for the flow problem

By using these suppositions, the governing equations [Malik et al. (2015)] are as follows:

Continuity equation

$$\frac{\partial (ru)}{\partial x} + \frac{\partial (rv)}{\partial r} = 0 \tag{3}$$

Momentum equation

$$\begin{aligned} &u\frac{\partial u}{\partial x} + v\frac{\partial u}{\partial r} = \nu\left(\frac{\partial^2 u}{\partial r^2} + \frac{1}{r}\frac{\partial u}{\partial r}\right) \\ &-\nu'\left(\frac{\partial^4 u}{\partial r^4} + \frac{2}{r}\frac{\partial^3 u}{\partial r^3} - \frac{1}{r^2}\frac{\partial^2 u}{\partial r^2} + \frac{1}{r^3}\frac{\partial u}{\partial r}\right) \\ &+\left(g\beta_1(T - T_\infty) + g\beta_2(T - T_\infty)^2\right)\cos\alpha \\ &-\frac{\nu}{k'}u - \frac{\sigma B_0^2}{\rho}u \end{aligned} \tag{4}$$

Energy equation

$$u\frac{\partial T}{\partial x} + v\frac{\partial T}{\partial r} = \frac{k}{\rho c_p}\frac{1}{r}\frac{\partial}{\partial r}\left(r\frac{\partial T}{\partial r}\right) \tag{5}$$

Concentration equation

$$\begin{aligned} u\frac{\partial a}{\partial x} + v\frac{\partial a}{\partial r} &= D_A\left(\frac{\partial^2 a}{\partial r^2} + \frac{1}{r}\frac{\partial a}{\partial r}\right) - l_1 ab^2 \\ u\frac{\partial b}{\partial x} + v\frac{\partial b}{\partial r} &= D_B\left(\frac{\partial^2 b}{\partial r^2} + \frac{1}{r}\frac{\partial b}{\partial r}\right) + l_1 ab^2 \end{aligned} \tag{6}$$

in which T is the fluid temperature, C is the fluid concentration, g is gravity, σ is the electrical conductivity, β_1 is thermal expansion coefficient, β_2 is non-linear thermal expansion coefficient, ν is kinematic viscosity, k is the thermal conductivity, ν' is couple stress viscosity, k' is the permeability of the porous medium, also assuming that both the chemical species A and B have equal diffusion coefficients D_A and D_B.

The pertinent boundary constraints are:

$$\begin{aligned} &at\ r = R,\ u = u_w(x) = \frac{U_0}{l}x,\ v = V,\ T \to T_w, \\ &D_A\frac{\partial a}{\partial r} = l_s a,\ D_B\frac{\partial b}{\partial r} = -l_s a \\ &at\ r \to \infty,\ u \to 0,\ \frac{\partial u}{\partial r} \to 0,\ \frac{\partial^2 u}{\partial r^2} \to 0, \\ &T \to T_\infty,\ a \to a_\infty,\ b \to b_\infty \end{aligned} \tag{7}$$

Now, we are introducing the similarity transformations [malik et al. (2015)] as follows:

$$\begin{aligned} &u = \frac{U_0}{l}xf'(\eta), \eta = \frac{r^2 - R^2}{2R}\left(\frac{U_0}{\nu l}\right)^{\frac{1}{2}}, \\ &v = -\frac{R}{r}\left(\frac{U_0\nu}{l}\right)^{\frac{1}{2}} f(\eta), \theta(\eta) = \frac{T - T_\infty}{T_w - T_0}, \\ &m(\eta) = \frac{a}{a_0}, n(\eta) = \frac{b}{a_0}, \text{where, } m(\eta) + n(\eta) = 1. \end{aligned} \tag{8}$$

By employing these dimensionless parameters (8), equations (2-7) are transformed into non-linear ODEs, expressed as follows:

$$\begin{aligned} &(1+2\gamma\eta)f''' + 2\gamma f'' + ff'' - f'^2 \\ &+(\theta + \gamma_1\theta^2)\lambda\cos\alpha - (d + M)f' \\ &-K\ \text{Re}\left[(1+2\gamma\eta)^2 f'''' + 8\gamma(1+2\gamma\eta)f''' + 8\gamma^2 f''\right] = 0 \end{aligned} \tag{9}$$

$$2\gamma\theta' + (1+2\gamma\eta)\theta'' - \text{Pr}(f'\theta - f\theta') = 0 \tag{10}$$

$$(1+2\gamma\eta)m'' + 2\gamma m' + Scfm' - ScLm(1-m)^2 = 0 \tag{11}$$

Reduced appropriate boundary constraints (7) are:

$$at\ \eta = 0,\ f(0) = -f_w,\ f'(0) = 1,\ \theta(0) = 1,$$
$$m'(0) = L_s m(0)$$
$$at\ \eta \to \infty, \qquad (12)$$
$$f'(\infty) = f''(\infty) = f'''(\infty) = \theta(\infty) \to 0,$$
$$m(\infty) = 1$$

Where,

$K = \frac{\nu'}{\nu R^2}$ Couple stress parameter,

$\mathrm{Re} = \frac{U_0 R^2}{\nu l}$ Reynolds number,

$d = \frac{\nu l}{U_0 k'}$ porosity parameter,

$\gamma = \left(\frac{\nu l}{U_0 R^2}\right)^{\frac{1}{2}}$ curvature parameter,

$\gamma_1 = \frac{\beta_2 (T_w - T_0)}{\beta_1}$ nonlinear temperature convection coefficient,

$\lambda = g(T_w - T_0)\beta_1 \frac{l^2}{U_0^2 x}$ combined convection parameter,

$M = \frac{\sigma B_0^2 l}{\rho U_0}$ magnetic field parameter,

$\mathrm{Pr} = \frac{\mu c_p}{k}$ Prandtl number,

$f_w = V\sqrt{\frac{l}{U_0 \nu}}$ suction/injection parameter,

$Sc = \frac{\nu}{D}$ Schmidt number,

$L = \frac{l_1 a_0^2 l}{U_0}$ homogeneous reaction parameter,

$L_s = \frac{l_s}{D_A}\sqrt{\frac{\nu l}{U_0}}$ heterogeneous reaction parameter

and the powers denote differentiation concerning η.

The non-dimensional forms of Skin-friction coefficient $C_f = \frac{2\tau_w}{\rho u_w^2}$, where $\tau_w = \mu\left(\frac{\partial u}{\partial r}\right)_{r=R}$, and Nusselt number $Nu = \frac{x q_w}{k(T_w - T_\infty)}$, where $q_w = -k\left(\frac{\partial T}{\partial r}\right)_{r=R}$ are $C_f = 2\mathrm{Re}_x^{-\frac{1}{2}} f''(0)$ and $Nu = -\mathrm{Re}_x^{\frac{1}{2}}\theta'(0)$ respectively, Where $\mathrm{Re} = \frac{U_0 x^2}{\nu l}$ denotes the local Reynolds number.

3. Method of Solution

The numerical solution for equations (9-11) affected by the boundary conditions (12) has been obtained using the RK-4 method in conjunction with a shooting technique. The chosen method requires a finite domain $0 \le \eta \le \eta_\infty$ and in this research, a domain of $\eta_\infty = 10$ has been selected.

In the first step, Let

$$\{f = f_1\};\ \{f' = f_2\};\ \{f'' = f_3\};\ \{f''' = f_4\};$$
$$\{f'''' = f_5\};\ \{\theta = f_6\};\ \{\theta' = f_7\};\ \{m = f_8\};$$
$$\{m' = f_9\}.$$

For these assumptions, the non-linear ODEs (9-11) are altered to first-order differential equations in the following form:

$$f_4' = \left\{\frac{1}{K\ \mathrm{Re}(1+2\gamma\eta)^2}\left\{\begin{array}{l}(1+2\gamma\eta)f_4 + 2\gamma f_3 - K\ \mathrm{Re}\left\{8\gamma(1+2\gamma\eta)f_5 + 8\gamma^2 f_4\right\} \\ +\lambda\left(f_6 + \gamma_1 f_6^2\right) - f_2(M + d) + f_1 f_3 - f_2^2\end{array}\right\}\right\}$$

$$f_7' = \left\{\frac{1}{(1+2\gamma\eta)}\left\{\mathrm{Pr}\left(f_2 f_6 - f_1 f_7\right) - 2\gamma f_7\right\}\right\}$$

$$f_9' = \left\{\frac{1}{(1+2\gamma\eta)}\left\{ScLf_8(1-f_8)^2 - 2\gamma f_8 - Scf_1 f_9\right\}\right\}$$

The boundary conditions (12) are reduced as

at $\eta = 0$, $f_1(0) = -f_w$, $f_2(0) = 1$, $f_6(0) = 1$, $f_9(0) = L_s f_8(0)$

at $\eta \to \infty$, $f_2(\infty) = f_3(\infty) = f_4(\infty) = f_6(\infty) \to 0$, $f_8(\infty) = 1$

We guess the values of f_3, f_7 and f_8, these are not given at initial conditions. Using step size 0.01, the process is continued, until we get the minimum error term.

4. Results and Discussion

The focus of this paper is to investigate the influence of chemical reactions on MHD couple stress fluid over an inclined stretching cylinder. The numerical solution is obtained using the Runge-Kutta approach with shooting technique. In this section, velocity, thermal, and concentration fields are analyzed against certain relevant parameters. The values of other parameters used to plot the graphs are taken as [Malik et al. [39]] $Pr = 1$, $\gamma = 1$, $K = 1$, $\lambda = 0.1$, $\gamma_1 = 0.1$, $M = 1$, $d = 0.1$, $Sc = 1.6$, $L = 0.1$, $L_s = 1$.

We have validated our results with Gajjela and Garvandha [2], for different values of γ and Pr (Table 1).

Figure (2) is plotted to show the velocity field exhibits a decrease as the couple stress parameter increases. This is attributed to the growth of couple stress viscosity with an increasing couple stress parameter, acting as a decelerating force leading to a denser fluid and consequently a reduction in the velocity field.

Figure (3) demonstrates the impact of the curvature parameter on the velocity field. Increasing the curvature parameter, results in a reduction in the cylinder radius, leading to a decrease in the contact area with the cylinder. Consequently, as γ increases, the velocity field near the surface of the cylinder decreases while it enhances farther away from the surface.

Figure (4) demonstrates that mixed convection has the effect of enhancing the velocity profile. As mixed convection grows, the buoyancy force dominates the viscous force that translates the flow from laminar to turbulent, which hastens the fluid flow.

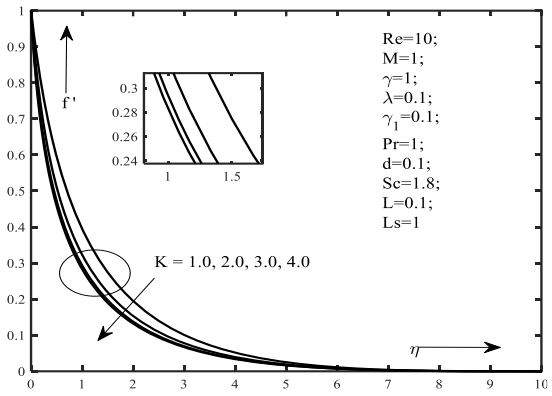

Fig. 2. Distribution of velocity for K

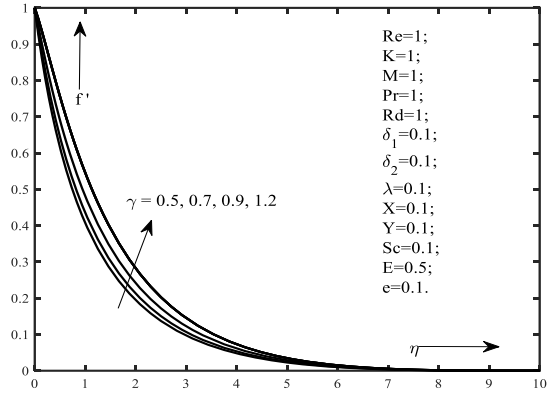

Fig. 3. Distribution of velocity for γ

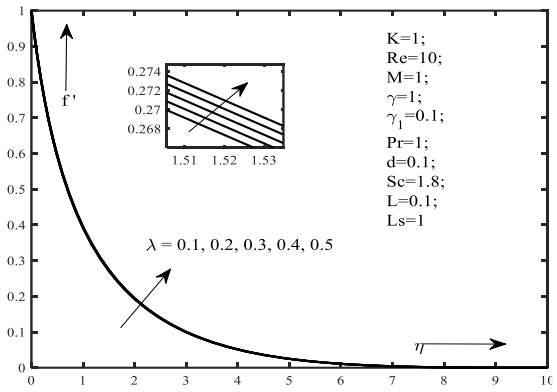

Fig. 4. Distribution of velocity for λ

Table 1. Comparison for value of $-f''(0)$ and $-\theta'(0)$

γ	$-f''(0)$		Pr	$-\theta'(0)$	
	Gajjela and Garvandha [2]	Present		Gajjela and Garvandha [2]	Present
0.0	1.61145	1.61157	0.7	0.1902	0.1905
0.05	1.62142	1.62176	1	0.2035	0.2042
0.1	1.63071	1.63066	1.3	0.2127	0.2133
0.15	1.63915	1.64120	1.5	0.2173	1.2282

Figure (5) depict the impact of the porosity parameter on the velocity field. An escalation in the porosity parameter indicates a greater presence of void spaces or pores within the medium. These empty spaces introduce increased resistance to the fluid flow, causing a decline in velocity. So, the velocity field experiences a decrease with an increase in the porosity parameter (d).

Figure (6) discerns that with an increase in the angle of inclination (α), the velocity field starts to decrease due to a reduction in the gravitational force. This occurrence can be understood by examining the gravitational forces acting both in alignment with and opposing the flow direction. When the angle of inclination is heightened, the effective gravitational force acting in the flow direction diminishes, resulting in a weakening of the force driving the fluid. Consequently, the velocity field, which indicates the speed and direction of fluid flow, undergoes a decline.

Figure (7) presented that the rising value of the magnetic parameter diminishes the velocity profile. Because the magnetic field is directed perpendicular to the cylinder axis, greater values of M amplify the Lorentz force, which, in turn, elevates the fluid's viscosity and subsequently diminishes the velocity distribution.

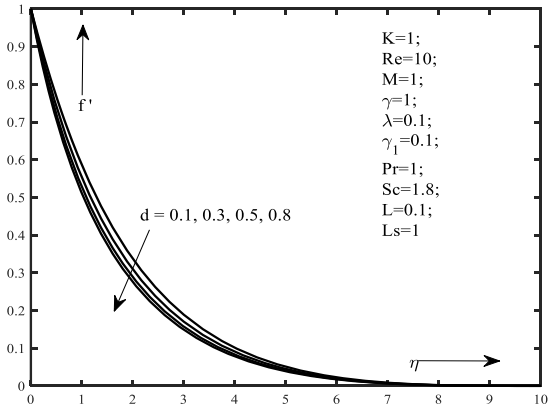

Fig. 5. Distribution of velocity for d

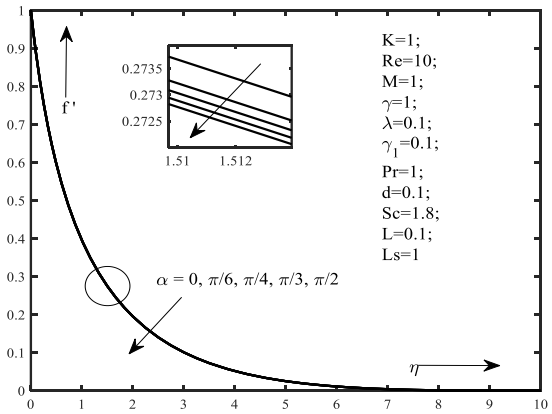

Fig. 6. Distribution of velocity for α

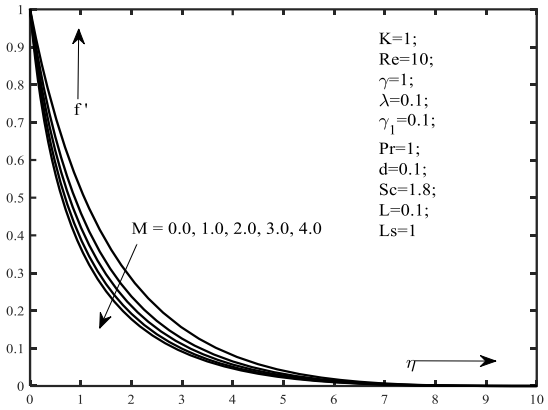

Fig. 7. Distribution of velocity for M

Figures (8-10) illustrate the impact of different parameters on thermal profiles. Figure (8) depicts the impact of the couple stress parameter on the thermal field. As the parameter of couple stress escalates, the viscosity of couple stress also goes up, causing the fluid to become denser. Consequently, this leads to a rise in the temperature profile.

Figure (9) depicts the impact of the curvature parameter on the thermal profile. As the curvature parameter γ rises, the cylinder radius reduces, causing a reduction in the fluid-cylinder contact area. This, in turn, leads to thicker thermal boundary layers with an increasing curvature parameter γ. Consequently, temperature profiles also rise as γ increases.

Figure (10) demonstrates the impact of the Prandtl number (Pr) on thermal profile. An upsurge in the Prandtl number leads to a reduction in the fluid's thermal diffusivity. The interplay among thermal conductivity, specific heat capacity, and density under constant pressure, termed thermal diffusivity, diminishes with higher Prandtl numbers. A lower thermal diffusivity triggers a decline in heat transfer rate, resulting in a reduction of the thermal boundary layer and, consequently, a decrease in the temperature field.

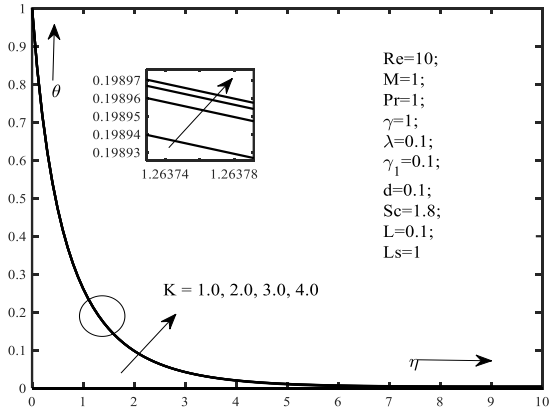

Fig. 8. Distribution of temperature for K

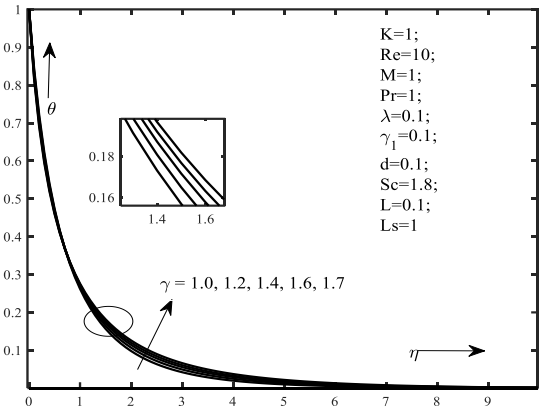

Fig. 9. Distribution of temperature for γ

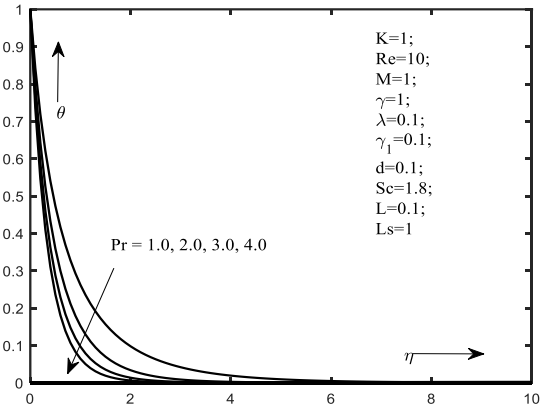

Fig. 10. Distribution of temperature for $\Pr$

Figures (11-12) shows the concentration profile is enhanced by increasing the value of the homogeneous-heterogeneous reactions parameter. As the homogeneous-heterogeneous reaction parameter rises, it signifies a heightened connection between reactions taking place in the homogeneous phase and those at the heterogeneous interfaces. This increased interaction results in a more complex dispersion of concentrations throughout the system; hence, the concentration profile increases.

Figure (13) is plotted to show the effect of Schmidt number on the concentration field. The Schmidt number quantifies the ratio between momentum diffusivity and mass diffusivity, providing a fundamental insight into the transport properties of a fluid system. Hence, mass diffusivity reduces on rising Schmidt number, which subsides the concentration profile. Figures (14-15) illustrates the variations in the skin friction coefficient and Nusselt number concerning the curvature parameter, mixed convection parameter, and Prandtl number. It is revealed in Figure (14) that the skin friction coefficient experiences an increase with the curvature parameter but decreases with the mixed convection parameter. Conversely, the Nusselt number demonstrates an enhancement for both the curvature parameter and Prandtl number, as observed in Figure (15).

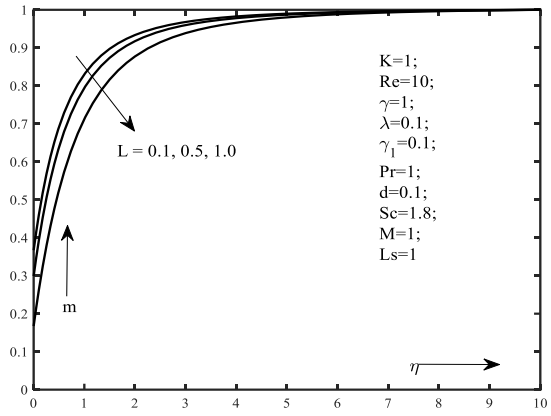

Fig. 11. Distribution of temperature for L

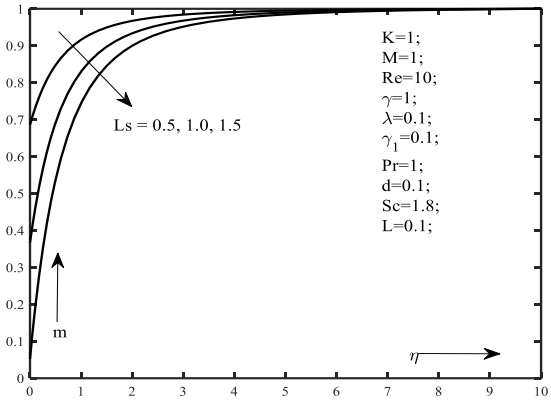

Fig. 12. Distribution of temperature for Ls

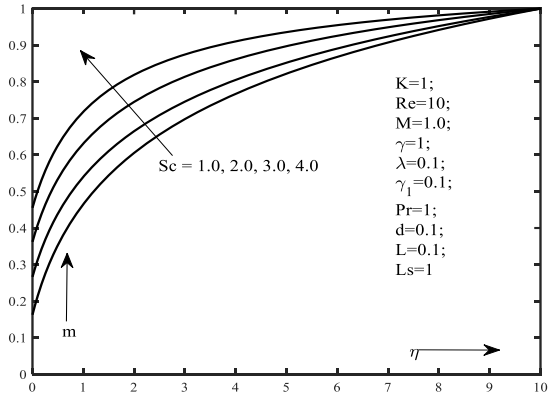

Fig. 13. Distribution of temperature for Sc

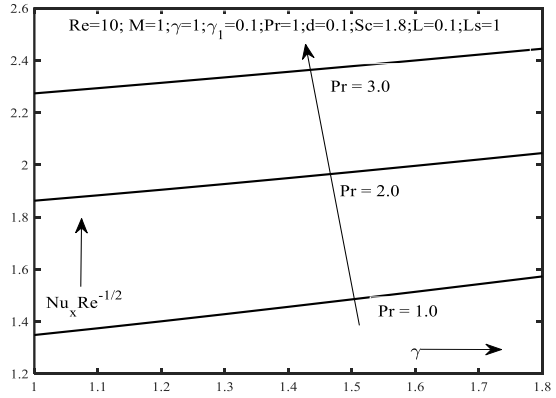

Fig. 14. Nusselt number for various value of γ and $\Pr$

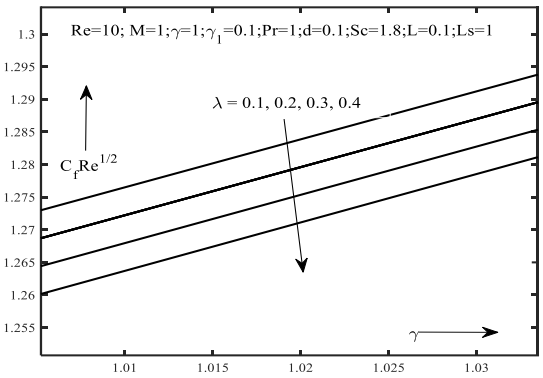

Fig. 15. Skin-friction coefficient for various value of γ and λ

5. Conclusions

A speculative study is done to investigate the influence of homogeneous-heterogeneous reactions on MHD viscous fluid with couple stress over an inclined stretching cylinder in the porous medium. The governing PDEs are evolved and transformed into ODEs by using adequate similarity alterations. These ODEs are subsequently solved using the shooting technique in conjunction with the fourth-order Runge-Kutta approach, implemented through MATLAB software. Then the following results are made:

Table 2. Numerical computation for coefficient of skin friction $f''(0)$; $\theta'(0)$ and $\phi'(0)$ for physical parameters

K	γ	d	M	Pr	L	Ls	Sc	$-f''(0)$	$-\theta'(0)$	$-m'(0)$
1								1.25422	1.34860	0.906061
2								1.25535	1.34909	0.906062
3								1.25580	1.34925	0.906063
4								1.25604	1.34932	0.906067
	1.2							1.40092	1.40100	0.88976
	1.4							1.53948	1.45639	0.87399
	1.6							1.67197	1.51387	0.86152
		0.3						1.24949	1.34937	0.906063
		0.5						1.24473	1.35015	0.906066
		0.8						1.23754	1.35132	0.906069
			0					1.27739	1.34481	0.906048
			2					1.23027	1.35251	0.906073
			3					1.20551	1.35653	0.906085
				2				1.25209	1.86308	0.906062
				3				1.25113	2.27411	0.906063
				4				1.25065	2.62086	0.906065
					0.5			1.254217	1.348601	0.90538
					1			1.254219	1.348602	0.89233
					1.5			1.254232	1.348604	0.86405
						0.5		1.25422	1.348606	0.45356
						1		1.25422	1.348606	0.90606
						1.5		1.25421	1.348607	1.35382
							2	1.254220	1.348608	0.906154
							3	1.254222	1.348612	0.906010
							4	1.254223	1.348615	0.905495

- As the couple stress parameter escalates, the velocity profile undergoes a reduction owing to the densification of the fluid, thereby instigating an upward trend in the temperature profile.
- Elevating the curvature parameter diminishes the contact area with the cylinder, fostering an enhancement in the velocity profile. Consequently, thicker thermal boundary layers emerge, fostering an augmentation in temperature profiles as γ increases.
- A rise in the convection parameter, instigates buoyancy force to overpower

viscous force, thereby amplifying the velocity profile.

- With the porosity parameter on the rise, the introduction of more void space amplifies the resistance to flow, thereby inducing a decline in the velocity profile.
- As the angle of inclination increases, a diminishing gravitational force prompts a decrease in the velocity field.
- Greater values of M intensify the Lorentz force, thereby augmenting the fluid's viscosity and consequently diminishing the velocity distribution.
- An escalation in the Prandtl number prompts a reduction in the fluid's thermal diffusivity, leading to a decrease in the heat transfer rate and, subsequently, a decline in the temperature field.
- The concentration field experiences a decline as homogeneous-heterogeneous reactions intensify, attributable to the heightened dispersion of concentrations across the system, resulting in a more intricate distribution pattern.
- With a rising Schmidt number, mass diffusivity diminishes, resulting in a subsiding concentration profile.

Nomenclature

A, B	Chemical species
B_0	Strength magnetic field (Wbm^{-2})
C_∞	Ambient concentration ($Kmol/m^3$)
c_p	Specific heat ($Jkg^{-1}K^{-1}$)
D_A, D_B	Diffusion coefficient of species A, B (m^2s^{-1})
d	Porosity parameter
f_w	Suction/injection parameter
g	Gravitational acceleration
K	Couple stress parameter
k	Thermal conductivity ($Wm^{-1}K^{-1}$)
k'	Permeability of the porous medium
L, L_s	Homogeneous, heterogeneous reaction strength
l	Characteristic length (m)
M	Magnetic field parameter
Pr	Prandtl number
Sc	Schmidt number
T_w	Temperature at surface (K)
T_∞	Ambient temperature (K)
u_w	Stretching velocity (ms^{-1})
V	Velocity of suction/injection

Greek symbols

ν'	Couple stress viscosity (m^2s)
σ	Electrical conductivity ($m^{-1}Ohm^{-1}$)
ρ	Density
γ	Curvature parameter
γ_1	Non-linear convection coefficient
λ	Combined convection parameter
α	Inclination of cylinder
β_1	Thermal expansion coefficient
β_2	Non-linear thermal expansion coefficient

Funding Statement

This research did not receive any specific grant from funding agencies in the public, commercial, or not-for-profit sectors.

Conflicts of Interest

The author declares that there is no conflict of interest regarding the publication of this article.

References

[1] Stokes, V. K., 1966. Couple stresses in fluids. *Phys. Fluids*, 9(9), pp. 1709–1715. doi: 10.1063/1.1761925.

[2] Rani, H. P., Reddy, G. J., Kim, C. N., 2011. Numerical analysis of couple stress fluid past an infinite vertical cylinder. *Eng. Appl. Comput. Fluid Mech.*, 5(2), pp. 159–169. doi: 10.1080/19942060.2011.11015360.

[3] Rani, H. P. and Reddy, G. J., 2013. Heatline visualization for conjugate heat transfer of a couple stress fluid from a vertical slender hollow cylinder. *Int. Commun. Heat Mass Transf.*, 48, pp. 46–52. doi: 10.1016/j.icheatmasstransfer.2013.08.015.

[4] Rani, H. P., Reddy, G. J., Kim, C. N., Rameshwar, Y., 2015. Transient Couple Stress Fluid Past a Vertical Cylinder with Bejan's Heat and Mass Flow Visualization for Steady-State. *J. Heat Transfer*, 137(3). doi: 10.1115/1.4029085.

[5] Ibrahim, W. and Gadisa, G., 2020. Double Stratified Mixed Convective Flow of Couple Stress Nanofluid past Inclined Stretching Cylinder Using Cattaneo-Christov Heat and Mass Flux Model. *Adv. Math. Phys.* doi: 10.1155/2020/4890152.

[6] Gajjela, N. and Garvandha, M., 2020. The influence of magnetized couple stress heat, and mass transfer flow in a stretching cylinder with convective boundary condition, cross-diffusion, and chemical reaction. *Therm. Sci. Eng. Prog.*, 18, p. 100517. doi: 10.1016/j.tsep.2020.100517.

[7] Palaiah, S. S., Basha, H., Reddy, G. J., 2021. Magnetized couple stress fluid flow past a vertical cylinder under thermal radiation and viscous dissipation effects. *Nonlinear Eng.*, 10(1), pp. 343–362. doi: 10.1515/nleng-2021-0027.

[8] Asad, S., Alsaedi, A. and Hayat, T., 2016. Flow of couple stress fluid with variable thermal conductivity. *Appl. Math. Mech.*, 37, pp. 315–324.

[9] Saeed, A., Kumam, P., Gul, T., Alghamdi, W., Kumam, W., Khan, A., 2021. Darcy–Forchheimer couple stress hybrid nanofluids flow with variable fluid properties. *Sci. Rep.*, 11(1), pp. 1–13. doi: 10.1038/s41598-021-98891-z.

[10] Bharty, M., Srivastava, A. K., Mahato, H., 2023. Stability of Magneto Double Diffusive Convection in Couple Stress Liquid with Chemical Reaction. *J. Heat Mass Transf. Res.*, 10(2), pp. 171–190. doi: 10.22075/jhmtr.2023.30246.1432.

[11] Malik R. and Khan, M., 2018. Numerical study of homogeneous–heterogeneous reactions in Sisko fluid flow past a stretching cylinder. *Results Phys.*, 8, pp. 64–70.

[12] Rashad, M. S., Manzoor, U., Khan, S. A., Liu, H., Muhammad, T., 2023. Numerical investigation of magnetized nanofluid flow with thermal radiation and homogeneous/heterogeneous reactions over a vertical cylinder. *Case Stud. Therm. Eng.*, vol., 50, p. 103424.

[13] Giri, S. S., Das, K., Kundu, P. K., 2020. Homogeneous-heterogeneous reaction mechanism on MHD carbon nanotube flow over a stretching cylinder with prescribed heat flux using differential transform method. *J. Comput. Des. Eng.*, 7(3), pp. 337–351. doi: 10.1093/jcde/qwaa028.

[14] Imtiaz, M., Mabood, F., Hayat, T., Alsaedi, A., 2019. Homogeneous-heterogeneous reactions in MHD radiative flow of second grade fluid due to a curved stretching surface. *Int. J. Heat Mass Transf.*,145, p. 11878.

[15] Jain, S. and Gupta, P., 2019. Second law analysis of MHD Casson and Maxwell fluid flow over a permeable stretching sheet with homogenous heterogeneous reactions and variable heat source. 57, pp. 385–399.

[16] Satya Narayana, P. V., Tarakaramu, N., Harish Babu, D., 2022. Influence of chemical reaction on MHD couple stress nanoliquid flow over a bidirectional stretched sheet. *Int. J. Ambient Energy*, 43(1), pp. 4928–4938.

[17] Naveed, M., Imran, M., Gul, S., 2023. Heat transfer analysis in hydromagnetic flow of couple stress fluid in presence of homogeneous and heterogeneous chemical reactions over a porous oscillatory stretchable sheet. *Adv. Mech. Eng.*, 15(2), p. 16878132231155824.

[18] Rana, S., Tabassum, R., Mehmood, R., Tag-eldin, E. M., Shah, R., 2024. Influence of Hall current & Lorentz force with nonlinear thermal radiation in an inclined slip flow of

couple stress fluid over a Riga plate. *Ain Shams Eng. J.*, 15(1), p. 102319.

[19] Swapna, D., Govardhan, K., Narender, G., Misra, S., 2023. Viscous Dissipation and Chemical Reaction on Radiate MHD Casson Nanofluid Past a Stretching Surface with a Slip Effect, *J. Heat Mass Transf. Res.*, 10(2), pp. 315–328. doi: 10.22075/jhmtr.2024.31758.1477.

[20] Kumari, M. and Jain, S., 2020. Radiative flow of MHD casson fluid between two permeable channels filled with porous medium and non-linear chemical reaction. *Int. J. Adv. Sci. Technol.*, 29(8), pp. 838–845.

[21] Parmar, A. and Jain, S., 2019. Influence of Non-Linear Chemical Reaction on MHD Convective Flow for Maxwell Fluid Over Three. 8(4), pp. 671–682. doi: 10.1166/jon.2019.1639.

[22] Abbas, N., Nadeem, S., Saleem, A., Malik, M. Y., Issakhov, A. and Alharbi, F. M., 2021. Models base study of inclined MHD of hybrid nanofluid flow over nonlinear stretching cylinder. *Chinese Journal of Physics*, 69, pp. 109–117.

[23] Awan, A. U., Ali, B., Shah, S. A. A., Oreijah, M., Guedri, K., Eldin, S. M., 2023. Numerical analysis of heat transfer in Ellis hybrid nanofluid flow subject to a stretching cylinder. *Case Stud. Therm. Eng.*, 49, p. 103222.

[24] Sohail, M. and Naz, R., 2020. Modified heat and mass transmission models in the magnetohydrodynamic flow of Sutterby nanofluid in stretching cylinder. *Phys. A Stat. Mech. its Appl.*, 549, p. 124088.

[25] Mabood, F., Yusuf, T. A., Bognár, G., 2020. Features of entropy optimization on MHD couple stress nanofluid slip flow with melting heat transfer and nonlinear thermal radiation. *Sci. Rep.*, 10(1), p. 19163.

[26] Afzal, Q., Akram, S., Ellahi, R., Sait, S. M., Chaudhry, F., 2021. Thermal and concentration convection in nanofluids for peristaltic flow of magneto couple stress fluid in a nonuniform channel. *J. Therm. Anal. Calorim.*, 144, pp. 2203–2218.

[27] Prasad, K. V., Choudhari, R., Vaidya, H., Bhat, A., Animasaun, I. L., 2023. Analysis of couple stress nanofluid flow under convective condition in the temperature-dependent fluid properties and Lorentz forces. *Heat Transf.*, 52(1), pp. 216–235.

[28] Mahat, R., Shafie, S., and Januddi, F., 2021. Numerical analysis of mixed convection flow past a symmetric cylinder with viscous dissipation in viscoelastic nanofluid. *CFD Lett.*, 13(2), pp. 12–28.

[29] Sun, S., Li, S., Shaheen, S., Arain, M. B., Usman, Khan K. A. A numerical investigation of bio-convective electrically conducting water-based nanofluid flow on the porous plate with variable wall temperature. *Numer. Heat Transf. Part A Appl.*, pp. 1–15. doi: 10.1080/10407782.2023.2242579.

[30] Fatima, N., Sooppy Nisar, K., Shaheen, S., Arain, M. B., Ijaz, N., Muhammad, T., 2023. A case study for heat and mass transfer of viscous fluid flow in double layer due to ciliated channel. *Case Stud. Therm. Eng.*, 45, p. 102943. doi: https://doi.org/10.1016/j.csite.2023.102943.

[31] Huang, H., Shaheen, S., Nisar, K. S., Arain, M. B., 2024. Thermal and concentration analysis of two immiscible fluids flowing due to ciliary beating. *Ain Shams Eng. J.*, 15(1), p. 102278. doi: https://doi.org/10.1016/j.asej.2023.102278.

[32] Arain, M. B., Zeeshan, A., Alhodaly, M. S., Fasheng, L., Bhatti, M. M., 2022. Bioconvection nanofluid flow through vertical rigid parallel plates with the application of Arrhenius kinetics: a numerical study. *Waves in Random and Complex Media*, pp. 1–18. doi: 10.1080/17455030.2022.2123115.

[33] Reddy, Y. D., Goud, B. S., Nisar, K. S., Alshahrani, B., Mahmoud, M., Park, C., 2023. Heat absorption/generation effect on MHD heat transfer fluid flow along a stretching cylinder with a porous medium. *Alexandria Eng. J.*, 64, pp. 659–666.

[34] Sudarmozhi, K., Iranian, D., Khan, I., 2023. Heat and mass transport of MHD viscoelastic fluid flow towards a permeable stretching cylinder. *Int. Commun. Heat Mass Transf.*, 145, p. 106864.

[35] Hussain, Z., Hayat, T., Alsaedi, A., Ullah, I., 2021. On MHD convective flow of

Williamson fluid with homogeneous-heterogeneous reactions: A comparative study of sheet and cylinder. *Int. Commun. Heat Mass Transf.*, 120, p. 105060.

[36] Arain, M. B., Zeeshan, A., Bhatti, M. M., Alhodaly, M. S., Ellahi, R., 2023. Description of non-Newtonian bioconvective Sutterby fluid conveying tiny particles on a circular rotating disk subject to induced magnetic field. *J. Cent. South Univ.*, 30(8), pp. 2599–2615. doi: 10.1007/s11771-023-5398-1.

[37] Sekhar, B. C., Kumar, P. V., Krishna, M.V., 2023. Changeable Heat and Mass Transport on Unsteady MHD Convective Flow Past an Infinite Vertical Porous Plate. *J. Heat Mass Transf. Res.*, 10(2), pp. 207–222. doi: 10.22075/jhmtr.2023.31618.1469.

[38] Chaudhary, M. A., Merkin, J. H., 1995. A simple isothermal model for homogeneous-heterogeneous reactions in boundary-layer flow. I Equal diffusivities. *Fluid Dyn. Res.*, 16(6), pp. 311–333. doi: 10.1016/0169-5983(95)00015-6.

[39] Malik, M. Y., Salahuddin, T., Hussain, A., Bilal, S., Awais, M., 2015. Homogeneous-heterogeneous reactions in Williamson fluid model over a stretching cylinder by using Keller box method. *AIP Adv.*, 5(10).